

# Conformal Symmetry and Pion Form Factor: Space- and Time-like Region

Ho-Meoyng Choi<sup>a</sup> and Chueng-Ryong Ji<sup>b</sup>

<sup>a</sup> Department of Physics, Teachers College, Kyungpook National University, Daegu, Korea 702-701

<sup>b</sup> Department of Physics, North Carolina State University, Raleigh, NC 27695-8202

We extend a recent analysis of the pion electromagnetic form factor constrained by the conformal symmetry to explore the time-like region. We show explicitly that the time-like form factor obtained by the analytic continuation of the space-like form factor correctly satisfies the dispersion relation. Our results indicate that the quark spin and dynamical mass effects are crucial to yield the realistic features of the vector meson dominance phenomena.

## I. INTRODUCTION

One of the most significant theoretical advances in recent years has been the application of AdS/CFT correspondence [1] between string theories defined on the 5-dimensional Anti-de Sitter(AdS) space-time and conformal field theories(CFT) in physical space-time. Although QCD is not itself a conformal theory, it may possess an approximate conformal symmetry in the domain where the QCD coupling is approximately constant and quark masses can be neglected. Based on the premise that QCD belongs to this class, theoretical development of AdS/CFT to QCD, often referred as “AdS/QCD” or “holographic QCD”, has been very popular in recent years. The resulting AdS/QCD model gives predictions for hadron spectroscopy [2] and a description of the quark structure of hadrons [3, 4] which has scale invariance and dimensional counting [5] at short distances, together with color confinement at large distances.

The AdS/QCD correspondence is particularly relevant for the description of hadronic form factors and also provides a convenient framework for analytically continuing the space-like results to the time-like region. The form factors have been studied within the holographic approach [3], and the connection between the AdS/QCD approach [3, 4] and the usual light-front formalism for hadronic form factors was proposed in [6] and discussed in [7]. Some other recent applications of different AdS/QCD models(hard-wall or soft-wall models)to the form factors of hadrons can be found in [8, 9, 10, 11, 12]. In AdS/QCD one breaks the conformal symmetry by impeding the ability of the field  $\Psi(x, z)$  to penetrate deeply into the bulk, which leads to an explanation of confinement and more generally constrains the model’s infrared(IR) behavior. This may be accomplished by imposing a hard cutoff and appropriate boundary conditions on  $\Psi(x, z)$  at some finite value of fifth dimension  $z = z_0$  [3](hard-wall model) or by imposing a soft IR cutoff with an oscillator-type potential in the action for large  $z$  [13](soft-wall model).

The connection between the AdS/QCD and the light-front approaches allows one to compute the analytic form of frame-independent light-front wavefunctions  $\psi_{n/h}$  of hadrons in physical space-time [6], thus providing a relativistic description of hadrons in QCD at the amplitude level. The pion electromagnetic form factor has been

exemplified by AdS/QCD, in particular, the power-law behavior of the form factor  $F_\pi(Q^2) \sim 1/Q^2$  is well reproduced by the soft-wall AdS/QCD model(or Gaussian model) [8]. The key ingredient in this correspondence is the conformal symmetry valid in the negligible quark mass. Using the connection between the AdS/QCD and the light-front approaches in the calculation of the hadronic form factors [8], we calculated [14] the pion form factor in our light-front quark model(LFQM) taking into account a momentum-dependent dynamical quark mass. We confirmed that the power-law behavior of the pion form factor is indeed attained by taking into account a momentum-dependent dynamical quark mass which becomes negligible at large momentum region. Our result [14] was consistent with an important point of AdS/QCD prediction, namely, the holographic wavefunction contains the contribution from all scales up to the confining scale. We also have shown that the broader shape of the pion distribution amplitude increases the magnitude of the leading twist perturbative QCD(PQCD) predictions for the pion form factor by a factor of 16/9 compared to the prediction based on the asymptotic form. Very recently, Brodsky and de Tera mond [10] extended their AdS/QCD model to obtain the time-like pion form factor by doing analytic continuation of the space-like result to the time-like region. However, the dispersion relation of the time-like form factor  $F(q^2) = \text{Re}F(q^2) + i\text{Im}F(q^2)$  has not yet been analyzed explicitly. We thus show in this work that the time-like form factor obtained by the analytic continuation of the space-like form factor correctly satisfies the dispersion relation. Working in the framework of the LFQM that takes into account a momentum-dependent dynamical quark mass [14], we further extend our previous analysis of the space-like pion form factor to the time-like region and compare with the result obtained from the AdS/QCD model [10]. Our comparative analysis reveals the effects from the quark spin and dynamical mass.

The paper is organized as follows. In Sec. II, we present the soft contribution to the pion form factor using the LFQM. In Sec. III, we present the space- and time-like pion form factor in the conformal symmetry limit. We also compare our LFQM results with the soft-wall AdS/QCD model calculation [10] to investigate the quark spin structure inside the pion. In Sec. IV, we show our numerical results of both space- and time-like

pion form factor. The direct calculation of the pion form factor is shown to be in excellent agreement with the result obtained from the dispersion relation. Summary and conclusion follow in Sec. V.

## II. PION FORM FACTOR IN LFQM

The elastic pion form factor is related to pion electromagnetic current by the following equation:

$$\langle P' | J^\mu(0) | P \rangle = (P' + P)^\mu F_\pi(Q^2). \quad (1)$$

As usual, our calculation will be carried out using the Drell-Yan-West frame ( $q^+ = q^0 + q^3 = 0$ ) where  $q^2 = (P - P')^2 = q^+ q^- - \mathbf{q}_\perp^2 = -Q^2$ , i.e.  $Q^2 > 0$  is the space-like momentum transfer. In this frame, the matrix element of the current can be expressed as convolution integral in terms of the light-front wavefunction and the pion form factor can be written for the “+”-component of the current  $J^\mu$  as follows (see [15] for more detailed calculation):

$$F_\pi(Q^2) = \int_0^1 dx \int d^2 \mathbf{k}_\perp \sqrt{\frac{\partial k_z}{\partial x}} \phi_R(x, \mathbf{k}_\perp) \sqrt{\frac{\partial k'_z}{\partial x}} \phi_R(x, \mathbf{k}'_\perp) \times \frac{m^2 + \mathbf{k}_\perp \cdot \mathbf{k}'_\perp}{\sqrt{m^2 + \mathbf{k}_\perp^2} \sqrt{m^2 + \mathbf{k}'_\perp^2}}, \quad (2)$$

where  $\mathbf{k}'_\perp = \mathbf{k}_\perp + (1-x)\mathbf{q}_\perp$  and the factors  $m^2$  and  $\mathbf{k}_\perp \cdot \mathbf{k}'_\perp$  in the numerator come from the ordinary helicity ( $\lambda + \bar{\lambda} = 0$ ) and the higher helicity ( $\lambda + \bar{\lambda} = \pm 1$ ) components of the spin-orbit wave function  $\mathcal{R}_{\lambda\bar{\lambda}}(x, \mathbf{k}_\perp)$ , respectively. Here, the explicit form of  $\mathcal{R}_{\lambda\bar{\lambda}}(x, \mathbf{k}_\perp)$  is obtained by the interaction-independent Melosh transformation [16] from the ordinary equal-time static spin-orbit wave function assigned by the quantum numbers  $J^{PC} = 0^{-+}$ . The radial wave function is given by

$$\phi_R(x, \mathbf{k}_\perp) = \sqrt{\frac{1}{\pi^{3/2} \beta^3}} \exp(-\vec{k}^2/2\beta^2), \quad (3)$$

where the gaussian parameter  $\beta$  is related with the size of pion and the three momentum squared  $\vec{k}^2$  can be represented by the light-front (LF) variables, i.e.

$$\vec{k}^2 = \frac{\mathbf{k}_\perp^2 + m^2}{4x(1-x)} - m^2, \quad (4)$$

for the quark mass  $m_u = m_d = m$ . For additional factor  $\sqrt{\partial k_z/\partial x}$  to the radial wavefunction  $\phi_R(x, \mathbf{k}_\perp)$  (similarly  $\sqrt{\partial k'_z/\partial x}$  to  $\phi_R(x, \mathbf{k}'_\perp)$ ) is the Jacobian of the variable transformation  $\{x, \mathbf{k}_\perp\} \rightarrow \vec{k} = (\mathbf{k}_\perp, k_z)$  due to the normalization of the radial wavefunction [17]. For the low momentum transfer phenomenology in LFQM, it is customary to take a constant constituent quark mass  $m$  as a mean value of the momentum dependent dynamical quark mass at low momentum region. The momentum dependence of the dynamical quark mass in

the spacelike momentum region has been discussed in lattice QCD [18] as well as in other approaches such as Dyson-Schwinger [19, 20] and instanton [21] models. Also, the difference between spacelike and time-like meson form factors at large momentum transfer was discussed in the framework of PQCD with Sudakov effects included [22]. Matching between the low momentum LFQM prediction and the large momentum PQCD prediction is a highly nontrivial task which goes beyond the scope of our present work. Nevertheless, as we discussed in [14], one should understand  $m$  as a function of  $Q^2$  in principle although in practice  $m(Q^2)$  for the low  $Q^2$  phenomenology can be taken as a constant constituent quark mass. In our previous analysis [14], we took the simple parametrization of the quark mass evolution  $m(Q^2)$  in space-like momentum region as  $m(Q^2) = m_0 + (m_c - m_0)(1 + e^{-0.2})/[1 + e^{(Q^2 - 0.2)}]$ , where  $m_0 = 5$  MeV and  $m_c = 220$  MeV represent the current (at high  $Q^2$ ) and constituent (at low  $Q^2$ ) quark mass, respectively. In this work, we take the same phenomenological form of  $m(Q^2)$  used in [14].

We note [14] that  $\phi_R(x, \mathbf{k}_\perp) \phi_R(x, \mathbf{k}'_\perp)$  in Eq. (2) provides a mass-dependent weighting factor  $e^{-\frac{m^2}{4x(1-x)\beta^2}}$  which severely suppresses the contribution from the endpoint region of  $x \rightarrow 0$  and 1 unless  $m \rightarrow 0$ . This weighting factor leads to the gaussian fall-off of  $F_\pi(Q^2)$  at high  $Q^2$  region for the constant constituent quark mass which breaks the conformal symmetry. When the conformal symmetry limit ( $m \rightarrow 0$ ) is taken, however, there is no such suppression of the endpoint region and the high  $Q^2$  behavior of the form factor dramatically changes from a gaussian fall-off to a power-law reduction. In the next section, we shall elaborate the pion form factor to explain why the power-law behavior attained in our Eq. (2) is not accidental but a consequence of the constraint taken from the conformal symmetry.

## III. SPACE- AND TIME-LIKE PION FORM FACTOR IN CONFORMAL SYMMETRY

In order to facilitate our calculation, we change the momentum variables as  $\mathbf{l}_\perp = \mathbf{k}_\perp + (1-x)\mathbf{q}_\perp/2$  and  $\xi^2 = (1-x)^2 \mathbf{q}_\perp^2/4$ . Then, the pion form factor (Eq. (2)) in the conformal symmetry limit ( $m \rightarrow 0$ ) is obtained as

$$F_\pi(Q^2) = \frac{1}{2\pi^{3/2} \beta^3} \int_0^1 dx \int_0^\infty d\mathbf{l}_\perp^2 \int_0^{2\pi} d\phi \mathcal{J} \mathcal{M} \times \exp\left[-\frac{\mathbf{l}_\perp^2 + \xi^2}{4\beta^2 x(1-x)}\right], \quad (5)$$

where  $\phi$  is the cosine angle between  $\mathbf{l}_\perp$  and  $\mathbf{q}_\perp$ . The Melosh factor  $\mathcal{M}$  coming from the spin structure of the pion and the product of two Jacobi factors  $\mathcal{J}$  are given by

$$\mathcal{M} = \frac{\mathbf{k}_\perp \cdot \mathbf{k}'_\perp}{\sqrt{\mathbf{k}_\perp^2} \sqrt{\mathbf{k}'_\perp^2}} = \frac{\mathbf{l}_\perp^2 - \xi^2}{\sqrt{(\mathbf{l}_\perp^2 + \xi^2)^2 - 4\mathbf{l}_\perp^2 \xi^2 \cos^2 \phi}}, \quad (6)$$

and

$$\mathcal{J} = \sqrt{\frac{\partial k_z}{\partial x}} \sqrt{\frac{\partial k'_z}{\partial x}} = \frac{[(I_\perp^2 + \xi^2)^2 - 4I_\perp^2 \xi^2 \cos^2 \phi]^{1/4}}{4[x(1-x)]^{3/2}}, \quad (7)$$

respectively. The exponential function in Eq. (5) comes from the product of two radial wave functions  $\phi_R(x, \mathbf{k}_\perp)$  and  $\phi_R(x, \mathbf{k}'_\perp)$ .

For the quark spin  $s = 1/2$  case, all of the factors  $\mathcal{J}$ ,  $\mathcal{M}$  and  $\phi_R(x, \mathbf{k}_\perp)\phi_R(x, \mathbf{k}'_\perp)$  should be kept in Eq. (5) and the pseudoscalar pion form factor respecting conformal symmetry ( $m = 0$ ) behaves as  $F_\pi^{s=1/2}(Q^2) \propto 1/Q^4$  at large  $Q^2$ . For the scalar quark ( $s = 0$ ) case, however, the Melosh factor is turned off (i.e.  $\mathcal{M} = 1$ ) and the corresponding pion form factor in the conformal limit ( $m = 0$ ) behaves as  $F_\pi^{s=0}(Q^2) \propto 1/Q^2$ . The latter case ( $F_\pi^{s=0}(Q^2) \propto 1/Q^2$ ) is shown [14] to be equivalent to the soft-wall AdS/QCD result at large momentum transfer [9, 10].

Let us now explore more of the spin and mass evolution effects to the pion form factor in space- and time-like regions. In the conformal limit ( $m = 0$ ) of the scalar quark (i.e.  $\mathcal{M} = 1$  in Eq. (5)) case, the form factor  $F_\pi^{s=0}(Q^2)$  after the  $\phi$ -integration has the following form

$$F_\pi^{s=0}(Q^2) = \frac{1}{4\beta^3 \sqrt{\pi}} \int_0^1 \frac{dx}{[x(1-x)]^{3/2}} \int_0^\infty dI_\perp^2 e^{-\frac{I_\perp^2 + \xi^2}{4\beta^2 x(1-x)}} \times \sqrt{I_\perp^2 + \xi^2} {}_2F_1\left(-\frac{1}{4}, \frac{1}{2}, 1; \frac{4I_\perp^2 \xi^2}{(I_\perp^2 + \xi^2)^2}\right), \quad (8)$$

where  ${}_2F_1(a, b, c; x)$  is the hypergeometric function with the range of convergence  $|x| < 1$  and  $x = 1$ , for  $c > a + b$ , and  $x = -1$ , for  $c > a + b - 1$ . Changing the variables in Eq. (8) as  $I_\perp^2 = \xi^2 \tan^2 \theta$  and  $4I_\perp^2 \xi^2 / (I_\perp^2 + \xi^2)^2 = \sin^2 2\theta$ , we obtain

$$F_\pi^{s=0}(Q^2) = \frac{(Q^2)^{3/2}}{16\beta^3 \sqrt{\pi}} \int_0^1 dx \left[\frac{1-x}{x}\right]^{3/2} \int_0^{\pi/2} d\theta g(\theta) \times e^{-\frac{(1-x)Q^2}{16\beta^2 x \cos^2 \theta}}, \quad (9)$$

where  $g(\theta) = (\sin \theta / \cos^4 \theta) {}_2F_1(-1/4, 1/2, 1; \sin^2 2\theta)$ .

After the  $x$ -integration, we could further reduce Eq. (9) to the following 1-dimensional form

$$F_\pi^{s=0}(Q^2) = \frac{(Q^2)^{3/2}}{16\beta^3} \int_0^{\pi/2} d\theta g(\theta) \times \left\{ \frac{(1+z)}{\sqrt{z}} - \frac{1}{2}(3+2z)e^z \Gamma\left(\frac{1}{2}, z\right) \right\}, \quad (10)$$

where  $z = Q^2/16\beta^2 \cos^2 \theta$  and  $\Gamma(\frac{1}{2}, z) = \sqrt{\pi} \text{Erfc}(z)$ . Here the incomplete gamma function,  $\Gamma(\frac{1}{2}, z)$ , has a branch cut discontinuity in the complex  $z$  plane running from  $-\infty$  to 0. This is the reason why the pion form factor is complex in time-like region ( $q^2 = -Q^2$ ) but real in space-like region. We now obtain the time-like form factor  $F_\pi(q^2)$  by

changing  $Q^2$  to  $-q^2$  in the form factor given by Eq. (10), where the imaginary part is obtained as

$$\text{Im}[F_\pi^{s=0}(q^2)] = \frac{(q^2)^{3/2} \sqrt{\pi}}{32\beta^3} \int_0^{\pi/2} d\theta g(\theta) (3 - 2z') e^{-z'}, \quad (11)$$

where  $z' = q^2/16\beta^2 \cos^2 \theta$ .

We find numerically that Eq. (8) is equivalent to the soft-wall AdS/QCD result in the large  $Q^2$  limit where the unconfined bulk-to-boundary propagator can be used [10], i.e.  $F_{(u.c.)}^{\text{AdS/QCD}}(Q^2) = \int_0^1 dx \exp[-(1-x)Q^2/4\kappa^2 x]$  (see Eq.(E.8) in [10]). This leads to the following analytic form in the space-like region

$$F_{(u.c.)}^{\text{AdS/QCD}}(Q^2) \simeq \frac{1 - e^{-\frac{Q^2}{4\kappa^2}} Q^2 \Gamma(0, \frac{Q^2}{4\kappa^2})}{4\kappa^2}, \quad (12)$$

where the subscript (u.c.) denotes the result of the unconfined current decoupled from the dilaton field. The imaginary part of the time-like  $F_{(u.c.)}^{\text{AdS/QCD}}(q^2)$  is given by

$$\text{Im}[F_{(u.c.)}^{\text{AdS/QCD}}(q^2)] = -\pi q^2 \frac{e^{-\frac{q^2}{4\kappa^2}}}{4\kappa^2}. \quad (13)$$

In the time-like region, the following dispersion relation should be satisfied

$$\text{Re}[F_\pi(q_0^2)] = \frac{1}{\pi} P \int_0^\infty \frac{\text{Im}[F_\pi(q^2)]}{q^2 - q_0^2} dq^2, \quad (14)$$

where  $P$  denotes the Cauchy principal value.

In our numerical calculation, we find that the equivalence between our  $F_\pi^{s=0}(Q^2)$  in conformal ( $m = 0$ ) limit and  $F_{(u.c.)}^{\text{AdS/QCD}}(Q^2)$  is achieved by matching our  $\beta = 0.173$  GeV with  $\kappa = 0.4$  GeV in [10] (i.e.  $\kappa \simeq 2.3\beta$ ). Comparing the gaussian dependence of our model wave function  $\Psi(x, \mathbf{k}_\perp) \sim \sqrt{\partial k_z / \partial x} e^{-\mathbf{k}_\perp^2 / 2(2\beta)^2 x(1-x)}$  in  $m = 0$  limit and the unconfined version of the soft-wall AdS/QCD model wave function  $\Psi(x, \mathbf{k}_\perp) \sim e^{-\mathbf{k}_\perp^2 / 2\kappa^2 x(1-x)} / \sqrt{x(1-x)}$  [10], we understand the relation between  $\beta$  and  $\kappa$  which is not exactly  $\kappa = 2\beta$  but  $\kappa \simeq 2.3\beta$  due to the different free factors. Other than such fine details, they are essentially equivalent to each other. The pion form factor in Eq. (12) respecting the conformal symmetry shows the power-law behavior of  $F_\pi(Q^2) \rightarrow 4\kappa^2/Q^2$  at large  $Q^2 (\gg \kappa^2)$ . The equivalence between our result without the Melosh factor in Eq. (8) and that of the soft-wall AdS/QCD model in the large  $Q^2$  limit given by Eq. (12) is assured when our LFQM respects the conformal symmetry.

We note that the authors in [10] also derived the pion form factor in the presence of a dilaton field in AdS space and presented the analytic solution of the modified wave equation for the confined bulk-to-boundary propagator. This corresponds to the well-known vector dominance model (VDM) with the leading  $\rho$  resonance, i.e.

$$F_{(confined)}^{\text{AdS/QCD}}(Q^2) = \frac{4\kappa^2}{4\kappa^2 + Q^2}. \quad (15)$$

In the timelike region, one may modify Eq.(15) to introduce a finite width (e.g.  $\Gamma = 100$  MeV in [10]) to compare with the pion form factor data near the  $\rho$  peak.

Although the analytic solution for the soft-wall unconfined current (Eq. (12)) is not much different from that for the soft-wall confined current (Eq. (15)) at large momentum transfer, the latter solution fits the low  $Q^2$  region much better than the former one. This implies that the dilaton background only affects the low  $Q^2$  region but shows the same  $1/Q^2$  power-law behavior of the pion form factor as that for the unconfined current. In our LFQM analysis, we consider both spin and mass evolution effects from the constituent quark and discuss the corresponding power-law behaviors in the pion form factor.

In order to see the spin effect on the pion form factor, we should include the Melosh factor  $\mathcal{M}$  given by Eq. (6). In this pseudoscalar ( $s = 1/2$ ) case, the pion form factor  $F_\pi^{s=1/2}(Q^2)$  given by Eq. (5) has the following form

$$F_\pi^{s=1/2}(Q^2) = \frac{1}{4\beta^3\sqrt{\pi}} \int_0^1 \frac{dx}{[x(1-x)]^{3/2}} \int_0^\infty d\mathbf{l}_\perp^2 e^{-\frac{\mathbf{l}_\perp^2 + \xi^2}{4\beta^2 x(1-x)}} \times \frac{\mathbf{l}_\perp^2 - \xi^2}{\sqrt{\mathbf{l}_\perp^2 + \xi^2}} {}_2F_1\left(\frac{1}{4}, \frac{1}{2}, 1; \frac{4\mathbf{l}_\perp^2 \xi^2}{(\mathbf{l}_\perp^2 + \xi^2)^2}\right), \quad (16)$$

after the  $\phi$ -integration. Following the same procedure as in the case of scalar pion case, we obtain the pseudoscalar pion form factor  $F_\pi^{s=1/2}(Q^2)$  in conformal limit by changing  $g(\theta)$  in Eq. (10) (and Eq. (11)) to  $g'(\theta) = -(\sin\theta \cos 2\theta / \cos^4\theta) {}_2F_1(1/4, 1/2, 1; \sin^2 2\theta)$ . We should note that the  $Q^2$  behavior of  $F_\pi^{s=1/2}(Q^2)$  is quite different from that of  $F_\pi^{s=0}(Q^2)$  since the  $\theta$  variable is related with the light-front momentum variables ( $x, \mathbf{k}_\perp$ ) as well as the momentum transfer  $Q^2$ . As discussed earlier, the pseudoscalar pion form factor behaves  $F_\pi^{s=1/2}(Q^2) \propto 1/Q^4$  at large  $Q^2$  compared to the scalar pion case,  $F_\pi^{s=0}(Q^2) = F_{(u.c.)}^{\text{AdS/QCD}}(Q^2) \propto 1/Q^2$ . In Fig. 1, we show the spin effect on the space- and time-like form factor respecting conformal symmetry ( $m = 0$ ) in the range of  $-2\text{GeV}^2 \leq Q^2 \leq 2\text{GeV}^2$ . Upper and lower panels represent the scalar ( $s = 0$ ) and pseudoscalar ( $s = 1/2$ ) pion cases, respectively. For a fixed  $Q^2$  value,  $\theta$  approaches to 0 and  $\pi/2$  for the low and high transverse momentum square  $\mathbf{k}_\perp^2$ , respectively. Fig. 1 reveals that the high  $\mathbf{k}_\perp^2$  region contributes more to the form factor than the low  $\mathbf{k}_\perp^2$  region. This feature is more enhanced by the spin effect as one can see from the comparison between the upper and lower panels of Fig. 1. Only after the  $\theta$  integration, we are able to check the dispersion relation between the real and imaginary parts of the form factor as we show in Fig. 5.

So far, we discussed the spin effect on the pion form factor in the conformal limit. In the rest of this section, we discuss the pion form factor given by Eq. (2) considering the momentum-dependent dynamical quark mass  $m(Q^2)$  used in our previous work [14]. Unlike the massless quark case, it is not so easy to analyze the time-like

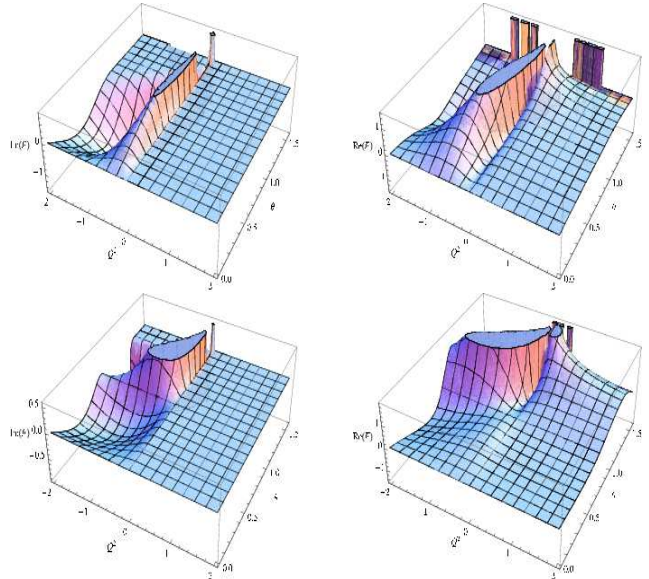


FIG. 1: Spin effect on the space- and time-like pion form factor respecting conformal symmetry ( $m = 0$ ) in the range of  $-2\text{GeV}^2 \leq Q^2 \leq 2\text{GeV}^2$ . Upper and lower panels represent the scalar ( $s = 0$ ) and pseudoscalar ( $s = 1/2$ ) pion cases, respectively.

region with Eq. (2) by doing analytic continuation due to the functional form of  $m(Q^2)$  taken. Nevertheless, as one can see from Fig. 2, we find that Eq. (2) with  $m = m(Q^2)$  is well approximated by the following analytic form up to intermediate space-like momentum transfer region:

$$F_\pi^{m(Q^2)}(Q^2) \simeq \frac{M_\rho^2}{Q^2 + M_\rho^2} F_\pi^{s=0}(Q^2), \quad (17)$$

where  $M_\rho$  is the physical mass of the  $\rho$  meson. For convenience, we shall call the right-hand-side of Eq. (17) as the modified soft-wall AdS/QCD result with  $\rho$  pole. We thus use the modified soft-wall AdS/QCD result with  $\rho$  pole as an approximate solution to the time-like pion form factor  $F_\pi^{m(q^2)}(q^2)$  with the dynamical quark mass. We should note in the calculation of the time-like pion form factor from Eq. (17) that  $M_\rho^2$  is replaced by  $\mathcal{M}_\rho^2 = M_\rho^2 - iM_\rho\Gamma(q^2)$  in the denominator where  $M_\rho = 776$  MeV and  $\Gamma = 120$  MeV to compare with the time-like pion form factor data near the  $\rho$  peak.

#### IV. NUMERICAL RESULTS

In this section, we compare our results for the space- and time-like form factor with the experimental data. We also show that our direct calculation of the time-like form factor obtained by the analytic continuation from the space-like region is in excellent agreement with that obtained from the dispersion relation.

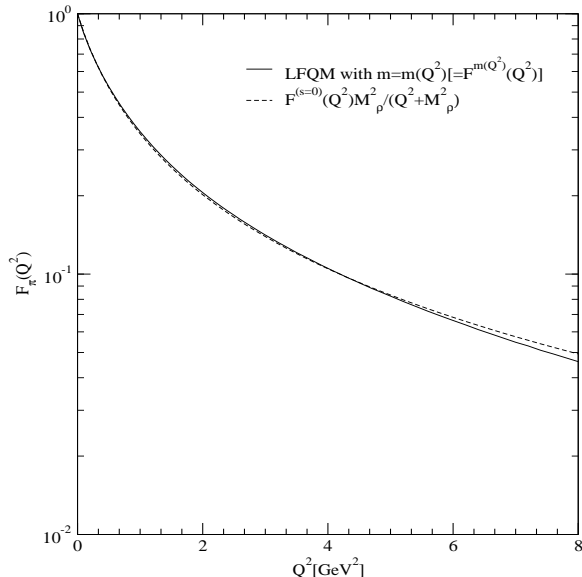


FIG. 2: Space-like pion form factor obtained from  $F_{\pi}^{m(Q^2)}(Q^2)$  [Eq. (2)] with the dynamical quark mass  $m(Q^2)$  (solid line) compared to the modified soft-wall AdS/QCD result [Eq. (17)] with  $\rho$  pole (dashed line).

The model parameters used in our numerical calculations are the followings:  $\beta = 0.173$  GeV for  $F_{\pi}^{s=0}(Q^2)$ ,  $\kappa = 0.4$  GeV for  $F_{(u.c.)}^{\text{AdS/QCD}}$  [9],  $\beta = 0.39$  GeV for  $F_{\pi}^{s=1/2}(Q^2)$  GeV and  $F_{\pi}^{m(Q^2)}(Q^2)$  (see [14] for the details of phenomenological form of the quark mass evolution), and  $\kappa = 3.2$  GeV for the modified AdS/QCD result with  $\rho$ -pole. With these model parameters, we are able to show the equivalences  $F_{\pi}^{s=0}(Q^2) \simeq F_{(u.c.)}^{\text{AdS/QCD}}(Q^2)$  and  $F_{\pi}^{m(Q^2)}(Q^2) \simeq \frac{M_{\rho}^2}{Q^2 + M_{\rho}^2} F_{\pi}^{s=0}(Q^2)$ . We obtain  $F_{\pi}^{m(Q^2)}(Q^2)$  by systematically taking into account the spin and quark mass evolution effects to  $F_{\pi}^{s=0}(Q^2)$  and verify the equivalence numerically modifying the form factor of the soft-wall unconfined current ( $F_{(u.c.)}^{\text{AdS/QCD}}(Q^2)$ ) with the empirical  $\rho$ -pole factor. We should note that the value of parameter  $\kappa$  in the modified soft-wall AdS/QCD result can be drastically different from that of  $F_{(u.c.)}^{\text{AdS/QCD}}(Q^2)$  due to the modification by the empirical  $\rho$ -pole factor. However, the physical observables are still comparable between the two models with and without the modification. For example, we obtain the pion decay constant  $f_{\pi} = 82.7$  MeV for  $F_{\pi}^{m(Q^2)}(Q^2)$  compared to 86.6 MeV for  $F_{(u.c.)}^{\text{AdS/QCD}}(Q^2)$  with  $\kappa = 0.4$  GeV.

In Fig. 3, we show the space-like behavior of  $Q^2 F_{\pi}(Q^2)$  for  $0 \leq Q^2 \leq 4$  GeV<sup>2</sup> region. The solid, dashed, dotted, and dot-dashed lines represent our LFQM result with the dynamical quark mass  $m(Q^2)$  in Eq.(2) (or equivalently modified soft-wall AdS/QCD model with  $\rho$ -pole in

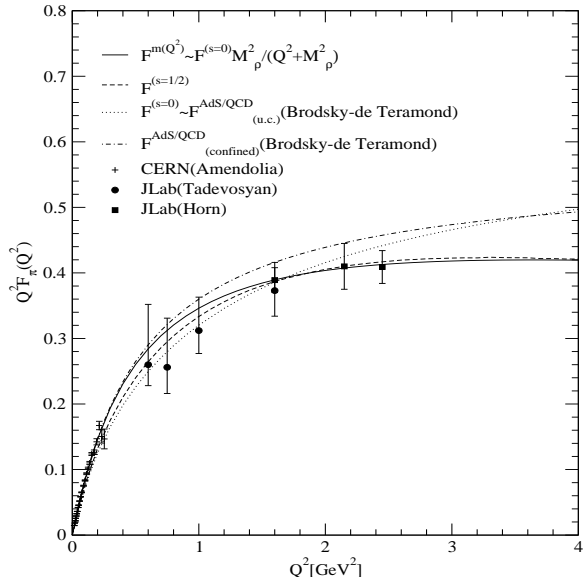


FIG. 3: Space-like behavior of  $Q^2 F_{\pi}(Q^2)$  for  $0 \leq Q^2 \leq 4$  GeV<sup>2</sup> region. Data are taken from [23, 24, 25, 26, 27].

Eq. (17)), the pseudoscalar pion form factor  $F_{\pi}^{s=1/2}(Q^2)$  with  $m = 0$ , the scalar pion form factor  $F_{\pi}^{s=0}(Q^2)$  with  $m = 0$  (or equivalently  $F_{(u.c.)}^{\text{AdS/QCD}}$  with the unconfined current in Eq. (12)), and the AdS/QCD result  $F_{(confined)}^{\text{AdS/QCD}}(Q^2)$  with the confined current in Eq. (15), respectively. Data are taken from [23, 24, 25, 26, 27], which includes the most recent results from JLAB [27]. While our previous LFQM result [14, 15] with constituent constant quark mass  $m = 220$  MeV shows the gaussian fall-off at high  $Q^2$  region, all the lines in Fig. 3 show the power-law behaviors at the available  $Q^2$  scale. Our  $Q^2 F_{\pi}^{m(Q^2)}(Q^2)$  with the dynamical quark mass (solid line) fits the data not only for the very low  $Q^2$  region but also for the intermediate  $Q^2$  region. Our  $Q^2 F_{\pi}^{s=1/2}(Q^2)$  (dashed line) is the result obtained by taking  $m = 0$  in  $Q^2 F_{\pi}^{m(Q^2)}(Q^2)$ . So the little difference between the two results shows the dynamical quark mass effect in the pion. Similarly, the difference between the result of the AdS confined current  $Q^2 F_{(confined)}^{\text{AdS/QCD}}$  (dot-dashed line) and that of the AdS unconfined current  $Q^2 F_{(u.c.)}^{\text{AdS/QCD}}(Q^2) \simeq Q^2 F_{\pi}^{s=0}(Q^2)$  (dotted line) in low  $Q^2$  region accounts for the effect of the dilaton field discussed in [10].

In Fig. 4, we show the space-like behavior of  $F_{\pi}(Q^2)$  for low  $0 \leq Q^2 \leq 0.3$  GeV<sup>2</sup> region. The same line codes are used as in Fig. 3. Our  $F_{\pi}^{m(Q^2)}(Q^2)$  (solid line) and  $F_{(confined)}^{\text{AdS/QCD}}(Q^2)$  (dot-dashed line) for this low momentum transfer region are not only very close to each other but also go through the data quite well. However, both  $F_{\pi}^{s=0}(Q^2)$  (i.e. soft-wall AdS/QCD model with the un-

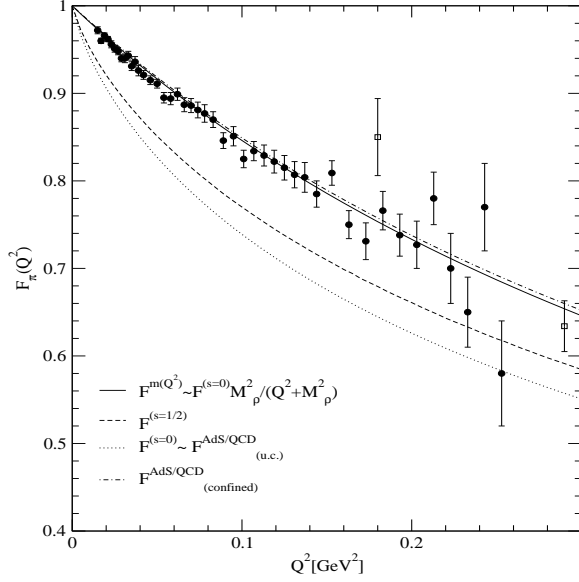


FIG. 4: Space-like behavior of  $F_\pi(Q^2)$  for  $0 \leq Q^2 \leq 0.3 \text{ GeV}^2$  region. Data are taken from [23, 24].

confined current) and  $F_\pi^{s=1/2}(Q^2)$  with  $m = 0$  overestimate the pion charge radius. From Figs. 3 and 4, we find that the low  $Q^2$  behaviors between  $F_\pi^m(Q^2)$  and  $F_{(confined)}^{AdS/QCD}(Q^2)$  are quite comparable to each other although the power-law behaviors at large momentum transfer region are different, i.e.  $F_\pi^m(Q^2)(Q^2) \sim 1/Q^4$  vs.  $F_{(confined)}^{AdS/QCD}(Q^2) \sim 1/Q^2$ . This may indicate a correspondence between the dilaton effect in AdS space and the spin and the mass evolution effects of constituent quark and anti-quark inside the pion.

In Fig. 5, we show the pion form factor for both space- and time-like region obtained from  $F_\pi^m(Q^2)(Q^2) \simeq \frac{M_\rho^2}{Q^2 + M_\rho^2} F_\pi^{s=0}(Q^2)$  (thick lines) and  $F_\pi^{s=0}(Q^2) \simeq F_{(u.c.)}^{AdS/QCD}(Q^2)$  (thin lines), respectively. The solid, dotted, and dashed lines represent  $|F_\pi(q^2)|$ ,  $\text{Re}[F_\pi(q^2)]$ , and  $\text{Im}[F_\pi(q^2)]$ , respectively. The black circles and squares are the results of  $\text{Re}[F_\pi^{s=0}(q^2)]$  and  $\text{Re}[F_\pi^m(q^2)]$  obtained from the dispersion relation given by Eq. (14). Fig. 5 shows that our direct calculations are in an excellent agreement with the solutions of the dispersion relation. Although  $F_\pi^{s=0}(Q^2)$  in time-like region produces a  $\rho$  meson-type peak near  $q^2 \sim M_\rho^2$  as in the case of our previous scalar field theory model [28], it does not yield all the features of the vector meson dominance phenomena as  $F_\pi^m(Q^2)(Q^2) \simeq \frac{M_\rho^2}{Q^2 + M_\rho^2} F_\pi^{s=0}(Q^2)$  does. This indicates that the spin and mass evolution effects are crucial in generating the more realistic features of the vector meson dominance phenomena.

In Fig. 6, we show the pion form factor for

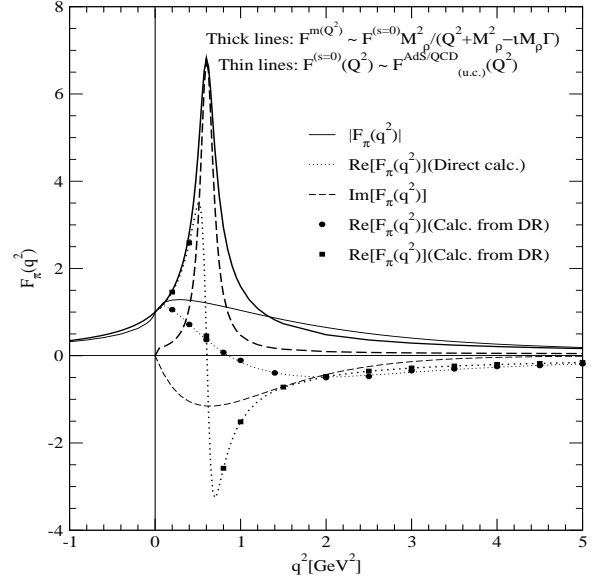


FIG. 5: Space- and time-like pion form factor obtained from  $F_\pi^m(Q^2)(Q^2) \simeq \frac{M_\rho^2}{Q^2 + M_\rho^2} F_\pi^{s=0}(Q^2)$  (thick lines) and  $F_\pi^{s=0}(Q^2) \simeq F_{(u.c.)}^{AdS/QCD}(Q^2) \text{ GeV}$  (thin lines) compared with the results obtained from the dispersion relation (black data).

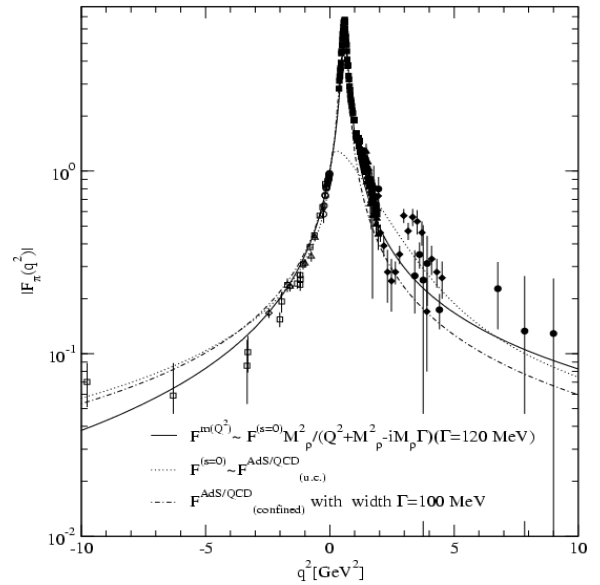


FIG. 6: Space- and time-like pion form factor obtained from  $F_\pi^m(Q^2)(Q^2) \simeq \frac{M_\rho^2}{Q^2 + M_\rho^2} F_\pi^{s=0}(Q^2)$  (solid line),  $F_\pi^{s=0}(Q^2) \simeq F_{(u.c.)}^{AdS/QCD}(Q^2) \text{ GeV}$  (dotted line), and  $F_{(confined)}^{AdS/QCD}(Q^2)$  (dash-dotted line), respectively. The data are taken from [23, 24, 25, 26, 27, 29, 30, 31, 32].

both space- and time-like region obtained from  $F_{\pi}^{m(Q^2)}(Q^2) \simeq \frac{M_{\rho}^2}{Q^2 + M_{\rho}^2} F_{\pi}^{s=0}(Q^2)$  (solid line),  $F_{\pi}^{s=0}(Q^2) \simeq F_{(u.c.)}^{\text{AdS/QCD}}(Q^2)$  GeV (dotted line), and  $F_{(confined)}^{\text{AdS/QCD}}(Q^2)$  [10] (dot-dashed line), respectively. The data in space- and time-like regions are taken from [23, 24, 25, 26, 27] and from [29, 30, 31, 32], respectively. As one can see from Fig. 6, our  $F_{\pi}^{m(Q^2)}(Q^2)$  and  $F_{(confined)}^{\text{AdS/QCD}}(Q^2)$  [10] exhibit more realistic  $\rho$  meson-type peak than  $F_{\pi}^{s=0}(Q^2)$ . Our LFQM analysis indicates that the difference between  $F_{\pi}^{m(Q^2)}(Q^2)$  and  $F_{\pi}^{s=0}(Q^2)$  is due to the spin (i.e. Melosh factor) and dynamical mass evolution effects of the constituent quark and anti-quark inside the pion. Our result may also be compared to the difference between  $F_{(confined)}^{\text{AdS/QCD}}(Q^2)$  and  $F_{(u.c.)}^{\text{AdS/QCD}}(Q^2)$ , which is due to the effect of the dilaton field in AdS space [10].

## V. SUMMARY AND CONCLUSION

We discussed a constraint of conformal symmetry in the analysis of the pion form factor. Working in the framework of the LFQM that takes into account a momentum-dependent dynamical quark mass [14], we ex-

tended our previous analysis of the space-like pion form factor to the time-like region and compared with the result obtained from the AdS/QCD model [10]. We showed explicitly that the time-like form factor obtained by the analytic continuation of the space-like form factor correctly satisfies the dispersion relation. Our comparative analysis between the scalar quark case ( $F_{\pi}^{s=0}(Q^2)$ ) and the spin 1/2 dynamical quark mass case ( $F_{\pi}^{m(Q^2)}(Q^2)$ ) indicates that the quark spin and dynamical mass effects are crucial to yield the realistic features of the vector meson dominance phenomena.

## Acknowledgments

We thank Stan Brodsky and Guy de Teramond for the useful discussion during the BARYONS07 International Conference and the subsequent correspondence. This work was supported by a grant from the U.S. Department of Energy (No. DE-FG02-96ER40947). H.-M. Choi was supported in part by Korea Research Foundation under the contract KRF-2005-070-C00039 and in part by Kyungpook National University Reserch Fund, 2007. The National Energy Research Scientific Center is also acknowledged for the grant of supercomputing time.

- 
- [1] J. M. Maldacena, *Adv. Theor. Math. Phys.* **2**, 231 (1998) [*Int. J. Theor. Phys.* **38**, 1113 (1999)]; S. S. Gubser, I. R. Klebanov, and A. M. Polyakov, *Phys. Lett. B* **428**, 105 (1998); E. Witten, *Adv. Theor. Math. Phys.* **2**, 253 (1998).
- [2] J. Erlich, E. Katz, D. T. Son, and M. A. Stephanov, *Phys. Rev. Lett.* **95**, 261602 (2005); H. Boschi-Filho and N. R. F. Braga, *JHEP* **0305**, 009 (2003); N. Evans and A. Tedder, *Phys. Lett. B* **642**, 546 (2006); D. K. Hong, T. Inami and H. U. Yee, *Phys. Lett. B* **646**, 165 (2007); P. Colangelo, F. De Fazio, F. Jugeau and S. Nicotri, *Phys. Lett. B* **652**, 73 (2007); H. Forkel, M. Beyer and T. Frederico, *JHEP* **0707**, 077 (2007).
- [3] J. Polchinski and M. J. Strassler, *Phys. Rev. Lett.* **88**, 031601 (2002); *JHEP* **0305**, 012 (2003).
- [4] S. J. Brodsky and G. F. de Teramond, *Phys. Lett. B* **582**, 211 (2004); G. F. de Teramond and S. J. Brodsky, *Phys. Rev. Lett.* **94**, 201601 (2005).
- [5] G. P. Lepage and S. J. Brodsky, *Phys. Rev. D* **22**, 2157 (1980).
- [6] S. J. Brodsky and Guy F. de Teramond, *Phys. Rev. Lett.* **96**, 201601 (2006).
- [7] A. V. Radyushkin, *Phys. Lett. B* **642**, 459 (2006).
- [8] G. F. de Teramond, Talk entitled “Mapping AdS/CFT Results for Holographic QCD to the Light Front” presented in the Workshop LC2006 (Light-Cone QCD and Nonperturbative Hadron Physics), Minneapolis, May 15-19, 2006; S. J. Brodsky, hep-ph/0608005 and hep-ph/0610115.
- [9] S. J. Brodsky and Guy F. de Teramond, arXiv:hep-ph/0702205.
- [10] S. J. Brodsky and Guy F. de Teramond, *Phys. Rev. D* **77**, 056007 (2008) (arXiv:0707.3859 [hep-ph]).
- [11] H. R. Grigoryan and A. V. Radyushkin, *Phys. Lett. B* **650**, 421 (2007); *Phys. Rev. D* **76**, 095007 (2007).
- [12] H. J. Kwee and R. F. Lebed, arXiv:0708.4054 [hep-ph]; arXiv:0712.1811 [hep-ph].
- [13] A. Karch, E. Katz, D. T. Son, and M. A. Stephanov, *Phys. Rev. D* **74**, 015005 (2006).
- [14] H. M. Choi and C. R. Ji, *Phys. Rev. D* **74**, 093010 (2006).
- [15] H.-M. Choi and C.-R. Ji, *Phys. Rev. D* **59**, 074015 (1999).
- [16] H. J. Melosh, *Phys. Rev. D* **9**, 1095 (1974).
- [17] H.-M. Choi and C.-R. Ji, *Phys. Rev. D* **56**, 6010 (1997).
- [18] J.I. Skullerud and A.G. Williams, *Phys. Rev. D* **63**, 054508 (2001); J.B. Zhang, P.O. Bowman, D.B. Leinweber, A.G. Williams and F.D.R. Bonnet, *Phys. Rev. D* **70**, 034505 (2004).
- [19] P. Maris and C.D. Roberts, *Phys. Rev. C* **58**, 3659 (1998).
- [20] P. Maris and P.C. Tandy, *Phys. Rev. C* **62**, 055204 (2000).
- [21] A. E. Dorokhov and L. Tomio, *Phys. Rev. D* **62**, 014016 (2000); A. E. Dorokhov, *Eur. Phys. J.C* **32**, 79 (2003).
- [22] T. Gousset and B. Pire, *Phys. Rev. D* **51**, 15 (1995).
- [23] C. J. Bebek *et al.*, *Phys. Rev. D* **17**, 1693 (1978).
- [24] S.R. Amendolia *et al.*, *Nucl. Phys. B* **277**, 168 (1986).
- [25] T. Horn *et al.*, *Phys. Rev. Lett.* **97**, 192001 (2006).
- [26] V. Tadevosyan *et al.*, nucl-ex/0607007.
- [27] T. Horn *et al.*, arXiv:0707.1794 [nucl-ex].
- [28] H.-M. Choi and C.-R. Ji, *Nucl. Phys. A* **679**, 735 (2001).
- [29] OLYA Collaboration, A. D. Bukin *et al.*, *Phys. Lett. B*

- 73**, 226 (1978).
- [30] OLYA and CMD Collaborations, L. M. Barkov *et al.*, Nucl. Phys. B **256**, 365 (1985).
- [31] DM2 Collaboration, D. Bisello *et al.*, Phys. Lett. B **220**, 321 (1989).
- [32] BCF Collaboration, D. Bollini *et al.*, Lett. Nuovo Cim. **14**, 418 (1975).